LAWRENCE
LIVERMORE
NATIONAL
LABORATORY

UCRL-JRNL-227806

Computational modeling of alloys at the atomic scale: from ab initio and thermodynamics to radiation-induced heterogeneous precipitation

A. Caro, M. Caro, P. Klaver, B. Sadigh, E. M. Lopasso, S. G. Srivilliputhur

February 6, 2007

Journal of the Minerals Metals and Materials Society

Disclaimer

Computational modeling of alloys at the atomic scale: from *ab initio* and thermodynamics to radiation-induced heterogeneous precipitation

A. Caro,[1] M. Caro,[1] P. Klaver,[2] B. Sadigh,[1] E. M. Lopasso,[3] and S. G. Srivilliputhur[4]

[1]*Chemistry, Materials, and Life Sciences Directorate, Lawrence Livermore National Laboratory, Livermore, CA 94550*
[2]*School of Mathematics and Physics, Queens University Belfast, Belfast BT7 1NN, Northern Ireland, United Kingdom*
[3]*Centro Atomico Bariloche - Instituto Balseiro. 8400 Bariloche, Argentina*
[4]*MST-8, Los Alamos National Laboratory, Los Alamos, NM 87545*

(Dated: November 30, 2006)

We describe the path we are following in the development of a computational approach to simulate radiation damage in FeCr ferritic steels. In these alloys magnetism introduces an anomaly in the heat of formation of the solid solution that has implications on the way excess Cr precipitates in the α' phase in presence of heterogeneities. These complexities represent a challenge for atomistic (empirical) approaches that we address *i*- by proposing a modified many body potential, *ii*- by using a thermodynamic package that determines free energy and phase diagrams, and *iii*- by using a displacement Monte Carlo code in the transmutation ensemble that can deal with millions of atoms in parallel computational environments. This approach predicts that grain boundaries, dislocations and free surfaces are not preferential sites for precipitation of α'.

The combination of quantum mechanics and thermodynamics/statistical mechanics is the paradigm on which quantitative computational materials science relies today. Accurate prediction of innumerable properties of the most diverse materials, comprising all kinds of constituents as well as time and space scales, is nowadays considered routine. However, both pillars have different strengths. While quantum mechanics has the power of an almost parameter-free theory for the potential energy landscape, as in for example Density Functional Theory (DFT), accurate estimates of various thermodynamic properties usually rely on sampling statistical ensembles using numerous approximations.

Many problems, frequently related to non-equilibrium properties, still cannot be addressed directly by the state of the art *ab initio* approach; approximations have to be used. Progress in computational capabilities and algorithm efficiency will not overcome these limitations in the foreseeable future. For that reason simplified models for the energetics are customarily used to capture partial aspects of reality, furthering our understanding of complex physical processes. For example, classical potentials are widely used for large scale dynamic simulations of a diversity of systems, in particular metals. At present classical interatomic potentials for real multicomponent materials show promising features for describing basic thermodynamic properties of such complex systems.

When mechanical properties and microstructure are the focus of attention, simulations have to be simple enough to allow dealing with a large number of atoms thus capturing the length scale that is relevant for this class of problems. The classical empirical total energy expressions that are so widely used have limitations to address real materials. In particular Fe alloys, the most commonly used materials for structural applications, continue to be a major challenge, as Fe is a complex element whose properties are determined by subtle features in its electronic structure. Impurities, intrinsic defects, and alloying elements in Fe play significant roles in determining its macroscopic mechanical properties. In nuclear reactors, structural components and fuel cladding undergo swelling and embrittlement as a consequence of radiation damage. The ability to perform atomistic computer simulations with predictive power for alloys in such environment is therefore a subject that has attracted the attention of the simulation community for a while.

FeCr alloys are commonly used as structural materials in present fission reactors. Due to their resistance to swelling, low ductile-to-brittle transition temperature, and their low activation properties, they are also being considered for use in future fusion reactors [1, 2]. High-energy particle bombardment will extensively damage the alloy. Displacement per atom (dpa) rates expected in fusion reactors are in the range of 100 [3], inducing microstructure evolution, swelling, and embrittlement.

In this article we describe the path we are following, and results we are getting, to understand some of the problems relevant for alloys for nuclear applications.

Figure 1 shows a schematic picture of our methodology: starting with data obtained either from *ab initio* calculations or from experimental measurements, we have developed a methodology linking this data to the formulation of empirical interatomic potentials, that can be used in large scale molecular dynamics (MD) simulations. It is the link labeled "1" in Figure 1. We target the relevant variables for the problem under consideration, for example the heat of formation (h.o.f.) of the alloys in the entire compositional range, the lattice parameter, or the elastic properties versus composition, etc, and develop a potential that reproduces these variables. Appendix I gives an overview of our procedure; further details can be found in Refs [4, 5]

The calculation of the thermodynamic properties of an alloy implies knowledge of the free energy of the relevant

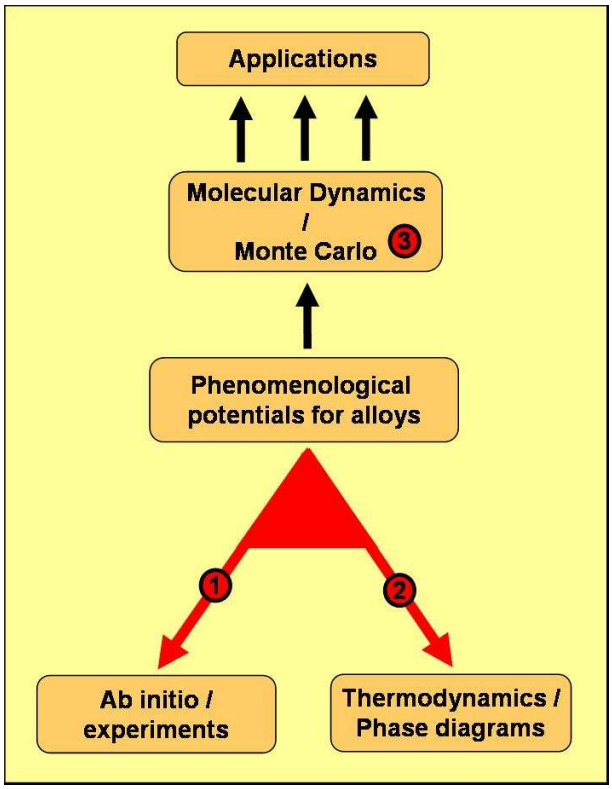

FIG. 1: Schematic picture showing the approach to describe alloy properties. Link number 1 represents the ability to develop classical potentials from data on formation energies of particular phases of the alloy of interest; link number 2 represents the ability to calculate thermodynamic functions of these potentials that can be compared to experiments or existing databases. Link number 3 represents the ability to do large scale Monte Carlo calculations on parallel computers where thermodynamic driving forces determine the outcome. The ensemble of these 3 capabilities allows us to calculate structures of FeCr alloys in heterogeneous environments like grain boundaries, dislocations, surfaces, cracks, etc.

phases as a function of composition and temperature. It is the link labeled "2" in Figure 1. The calculation of the free energy is a multi-step process that requires a series of MD runs. We have recently implemented a numerical package that efficiently and accurately calculates free energies. For a complete description of the method we refer the reader to several previous publications [4–8]. Here we only highlight its basic aspects, together with the main equations; see appendix II.

Following the methodology proposed in CALPHAD [9] we separate the problem of binary alloys into the properties of the pure elements (i. e. the free energies of all possible phases of the pure elements) and the properties of the mixtures. The latter are expressed in terms of excess enthalpy and entropy. Excess quantities are referred to the linear interpolation between the pure elements, which represents the ideal solution. In this way the alloy description is conveniently separated into two distinct parts: the description of the pure elements on the one hand, and the description of the mixture on the other. The CALPHAD approach is a standardized way to express the thermodynamic information of a system. Once the free energies are expressed in this way (suggested by the Scientific Group Thermodata Europe (SGTE) [10]) the calculation of phase diagrams can easily be performed with an application software such as Thermo-Calc [9].

Our numerical results can be compared with those from a thermodynamic database that contains generally accepted values for these quantities, taken from Dinsdale's compilation [11]. The latter constitute for us what we take as experimental values although not all data in the database are from experimental assessment. In this work, we use the Fe potential reported by Mendelev *et al.* [12] and the Cr potential reported by Wallenius *et al.* [13]. The formation energy for FeCr has recently been calculated by Olsson *et al.* [14] together with a rough estimate of the bulk modulus and lattice parameter of the alloy as a function of composition. These calculations, albeit *ab initio*, still contain several simplifications, and are therefore not to be considered as definitive, but as first estimates based on which classical models can be developed.

In a recent paper, Klaver *et al.* [15] used DFT calculations to study the mixing behavior of FeCr alloys. They confirm the previous observations by Olsson et al. [14] and by Mirzoev et al. [16] regarding the change in sign in the

formation energy of the alloy at $x \sim 0.1$ (in what follows, x refers to Cr composition). The subtle electronic structure that arises when ferromagnetic (fm) and antiferromagnetic (afm) metals are mixed in different ratios is considered as the origin of this anomaly. In fact, magnetic frustration leads to a strong dependence of the Cr moment on the number of Cr neighbors. Magnetic frustration occurs when it is impossible for an Fe or a Cr atom to assume a fm or afm state respectively, with respect to all its neighbors. This translates into a repulsive interaction that competes with the large negative heat of solution of a single Cr impurity, i. e. a tendency to form ordered compounds. The limitations of the quasi-chemical description for the energetics of this system (see Appendix 2) become readily apparent when we realize that in an expression like Eq. 1 in Appendix I the Cr-Cr interaction has to be attractive since Cr is in a condensed phase at 0 K, while it becomes repulsive when the Cr-Cr pair is surrounded by Fe. It implies then that a pair like model for the energetics has to contain explicit composition dependent terms.

As a first test of our approach, we compare classical and *ab initio* calculations of the Cr-Cr interaction when a Cr substitutional pair is embedded in an otherwise pure Fe matrix and their separation distance is increased, see Figure 2. Apart from the fine structure of the *ab initio* results at the fifth-neighbor separation, attributed to finite size effects [15], the agreement in both strength ($\sim$ 300 meV) and range ($\sim 2.2a_0$) of the interaction is very good, giving support to this classical model as being able to capture the Cr-Cr pair repulsion aspects of the energetics in this system.

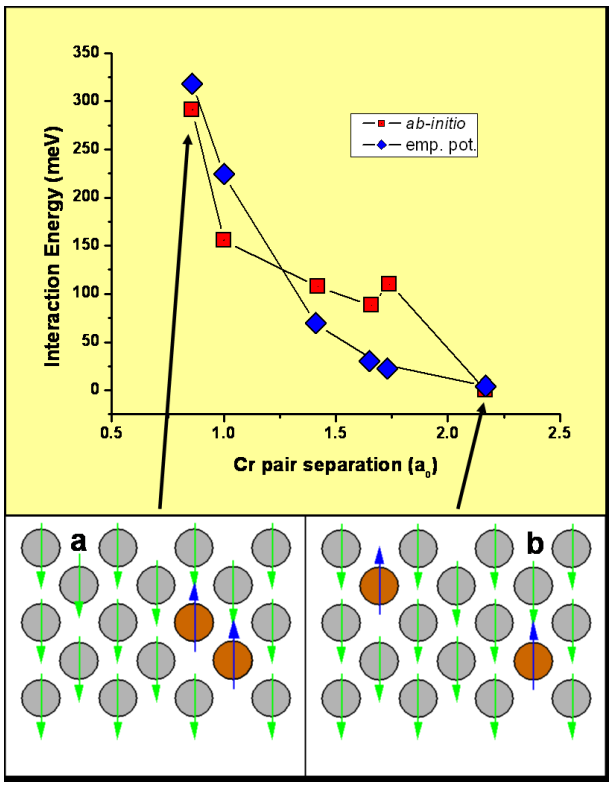

FIG. 2: Upper part: Interaction energy of two substitutional Cr atoms in a Fe matrix versus separation distance. Squares are *ab initio* results from [15], diamonds are obtained with the empirical potential [17]. Lower part: schematic representation of the magnetic frustration occurring at short Cr-Cr distances, preventing energetically favorable moment alignment.

A more stringent test of the potential is to compare the energy dispersion between different configurations of Cr substitutionals at a given global composition and sample size. Because *ab initio* calculations involve small supercells, disordered configurations always represent ordered supercell structures with image interactions translating into significant dispersion of the results. On the other hand, simulations based on empirical potentials can afford large system sizes and thus many possible local configurations of random solutions are adequately explored, which translates into small energy dispersion between different realizations of the random samples. It should be noted here that the *ab initio* results by Olsson [14] used by us to derive our classical potential do not have dispersion because they are obtained using the Coherent Potential Approximation, a mean field methodology for disordered alloys.

The *ab initio* results that we are going to compare with ours were obtained in supercells of 16, 24, and 54 atoms. These numbers are too small for the EAM formalism (minimum size is twice the cutoff of the interactions, involving $\sim$ 100 atoms). We therefore replicated the *ab initio* 54 atom sample 3x3x3 times to get the classical 1458 atoms

sample, and 4x4x4 times for the smaller ones. While this procedure reproduces some of the finite size constraints appearing in the *ab initio* calculations, it still allows for relaxations with wavelengths equal to 3 or 4 times the size of the *ab initio* supercell, not accounted for in the *ab initio* calculations; some discrepancies are therefore expected. Finally, since our classical potential is fitted to the h.o.f. by Olsson, and the results by Klaver use a different *ab initio* approach, the comparison is done not in absolute values but in dispersion around a mean. Figure 3 shows several cases, at different compositions and cell sizes. The agreement in the range of the dispersion between different configurations goes from surprisingly good in some cases to reasonably good in others, within the accuracy of the calculations. From Figures 2 and 3 we conclude that the complexity of the interactions in the solid solution is reasonably well captured by our classical potential.

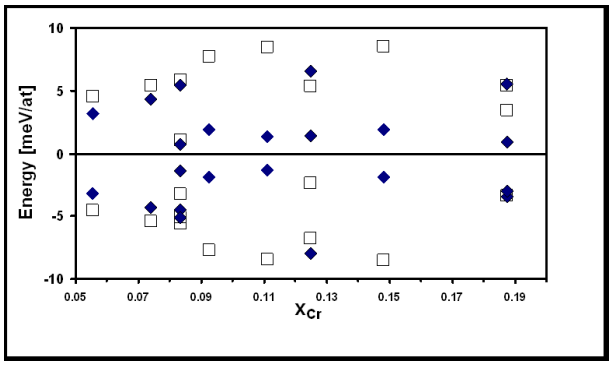

FIG. 3: Comparison of relative energy differences in several FeCr configurations explored in [15]. Diamonds represent *ab initio* calculations and squares represent classical potential results on the same samples. For a discussion see text.

The above tests provide support for our approach to represent the interactions in the alloy. Now we turn to thermodynamic properties. From the free energy function represented in Figure 10 in Appendix II we obtain the miscibility gap and the spinodal, see Figure 4. For comparison, we also show in the figure the *solvus* as it appears in SSOL, the database of CALPHAD [9]; note that all other crystal phases have been omitted. Several differences are readily noticeable. Neither the miscibility gap nor the spinodal go to zero composition at 0 K on the Fe rich side of the diagram. This curious effect is due to the change in the sign of the h.o.f. of this alloy at about 10%, which implies finite solubility at low temperatures. Additionally, the critical temperature for our *ab initio* plus classical thermodynamics model is much higher ($\sim$ 1300 K) than the value in the SSOL data. The reason is that the h.o.f. data of Olsson [14], on which our potential is based, shows a maximum of about 100 meV, a value well above the SSOL data (60 meV); on the other hand, excess vibrational entropies agree very well. For details see [5]

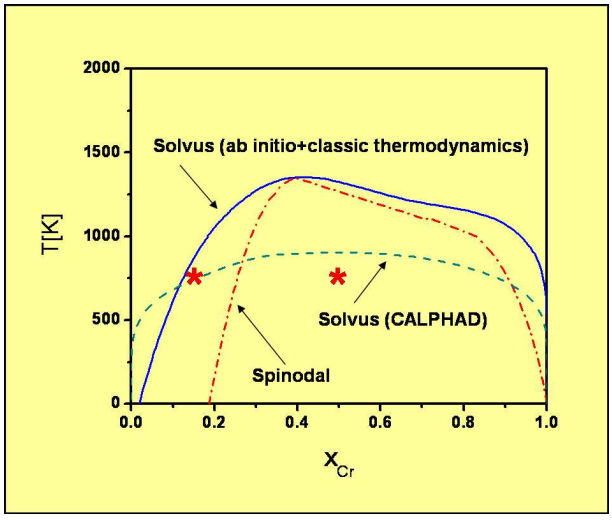

FIG. 4: Miscibility gap and spinodal of the ferromagnetic phase of the FeCr solid solution as obtained from the free energy in Figure 10. Also shown is the *solvus* as it appears in SSOL, the database of CALPHAD [9]. Note the finite solubility of Cr in Fe at low Cr compositions and low T. In this region, ordered phases should exist. Stars represent the alloys studied in Figures 6 and 7

To describe non-equilibrium processes in heterogeneous systems with defects and external potentials, a new computational tool is needed. Most computational approaches to non-equilibrium are based on kinetic Monte Carlo (MC) algorithms that in one way or another have to adopt a frozen backbone or lattice where the diffusing species jump. This is a necessary restriction because a time tracking algorithm needs rates for all possible events [18].

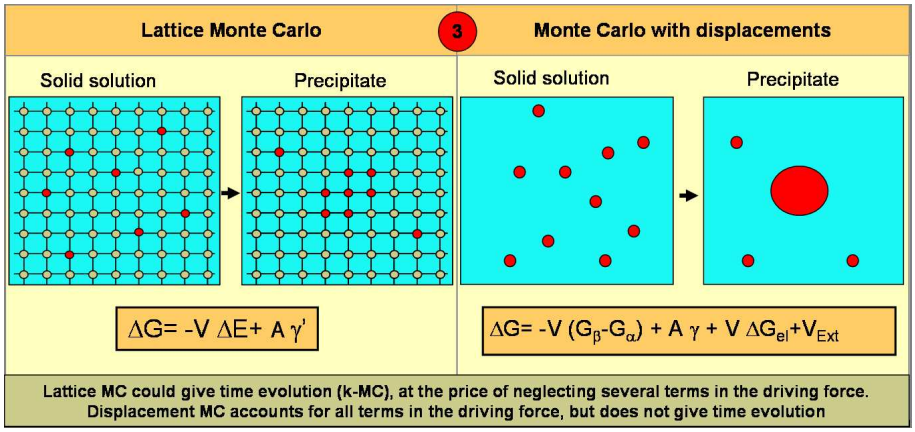

FIG. 5: Schematic representation of the parallel Monte Carlo code with displacement used in this work, showing the differences in the driving forces (ΔG) between a lattice algorithm and a displacement algorithm. See also text.

Kinetics and thermodynamics are two aspects of the problem of evolution in non-equilibrium systems [19]. Since one cannot yet treat both at the same level of accuracy, one has to choose which one is more relevant for the problem under consideration. Here we focus on thermodynamics, with a parallel MC code that drives the system, with no approximations to the potential energy landscape, towards thermodynamic equilibrium by minimizing the free energy as MC steps go on. Figure 5 shows a schematic representation of this algorithm. Details will be published elsewhere [20]. While the driving force for a lattice algorithm is the difference in energy between the two phases plus a contribution from a simplified interface energy, the displacements algorithm accounts for all terms with no approximations: differences in free energy between the phases, actual interfacial free energy, the contribution from elastic energy created by lattice mismatch, and interaction with external potentials (external or internal stress fields, originating in defects like grain boundaries, cracks, dislocations, surfaces, etc).

We use the above methodology to study homogeneous precipitation of α' phase in saturated FeCr solution. We start with the homogeneous case at two compositions, $x = 0.15$ and $x = 0.5$, at $T = 750$ K, points identified with stars in Figure 4. These points in the phase diagram are shown as red stars in Figure 4; $x = 0.15$ is just above the solubility limit, while $x = 0.5$ is well within the spinodal. Figure 6 shows 2D slice sequences from MC simulations that represent steps towards equilibrium, starting from a solid solution and evolving towards a state with the sample separated into regions of α and α'. All three simulations correspond to perfect crystal cubic samples with $\sim$2 millon atoms and periodic boundary conditions. Frames a-d show homogeneous precipitation and coarsening of α'. The fact that Cr-Cr interaction is repulsive implies that there is a critical size for the nuclei to be stable; and the fact that the decomposition mechanism at this concentration is nucleation and growth implies that the concentration of the nuclei is always the saturation composition of α', i. e. $x \cong 0.99$. As MC steps go on, the precipitates adopt a spherical shape, indicative of small anisotropy on the interface energy. Panels e-h focus on one particular precipitate, highlighting the fact that there is a critical size below which there are no stable precipitates, and the evolution to spherical shape. Panels i-l show evolution of the alloy via spinodal decomposition, i. e. continuous increase of composition differences from $x = 0.5$ to the terminal solution values $x = 0.12$ for α and $x = 0.99$ for α'.

We now analyze the case of heterogeneous precipitation, i. e. precipitation in the presence of defects. We choose to explore this process in a polycrystalline sample with average grain size of 5 nm. This way we can observe a multiplicity of configurations of grain boundaries, triple and higher order junctions, and eventually surfaces, in a single run. Figure 7 shows four slices taken at different locations in a cubic sample represented by the boxes in the figure; simulation parameters are $x = 0.15$ and $T = 750$ K. Blue dots are Fe atoms sitting at boundaries, red dots are Cr atoms. Fe atoms at perfect bcc positions are not shown. A surprising effect can readily be observed: excess Cr does not precipitate at boundaries, instead all α' precipitates are in the interior of the grains, avoiding contact with the grain boundary network.

FeCr ferritic steels are candidate materials for diverse applications in advanced nuclear energy systems, from cladding of fuel to structural components. Recent *ab initio* results have shown that magnetism in these alloys plays an important role in determining its energetics at 0 K. In this work we develop an approach to computationally model processes

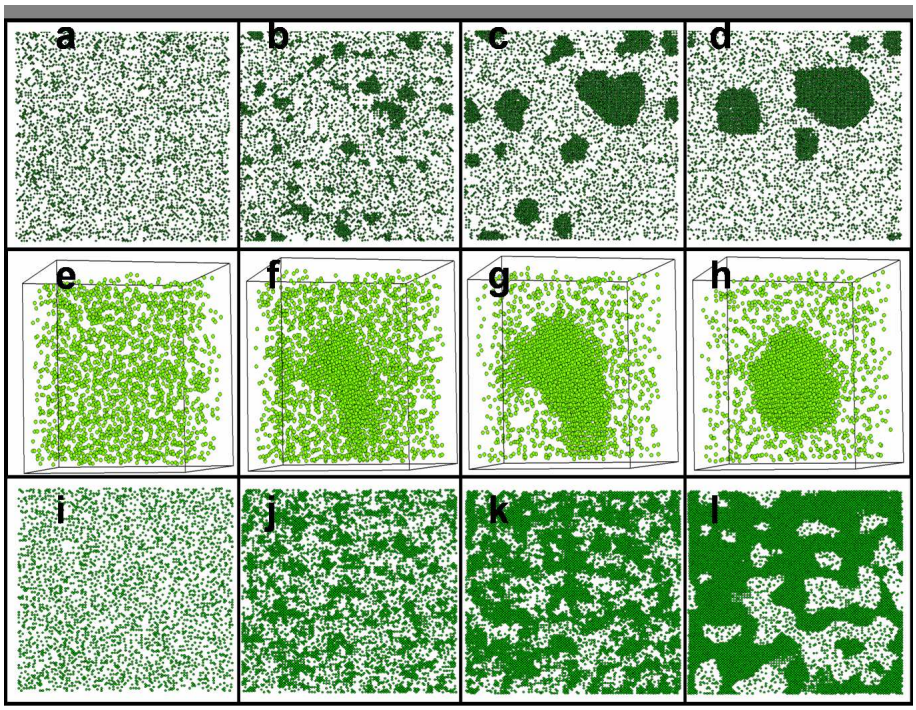

FIG. 6: 2D slice sequences along three MC simulations starting from a solid solution and evolving towards thermodynamic equilibrium. Frames a-d show homogeneous precipitation and coarsening of α'. There is a critical size for the nuclei to be stable; the concentration of the nuclei is always the saturation composition of α', i. e. $x \sim 0.99$. As MC steps go on, the precipitates adopt a spherical shape. Frames e-h show one particular precipitate highlighting the fact that there is a critical size below which there are no stable precipitates and the evolution to spherical shape. Panels i-l show evolution of the alloy via spinodal decomposition, i. e. continuous increase of composition differences from $x = 0.5$ to the terminal solution values of $x = 0.12$ for α and 0.99 for α'.

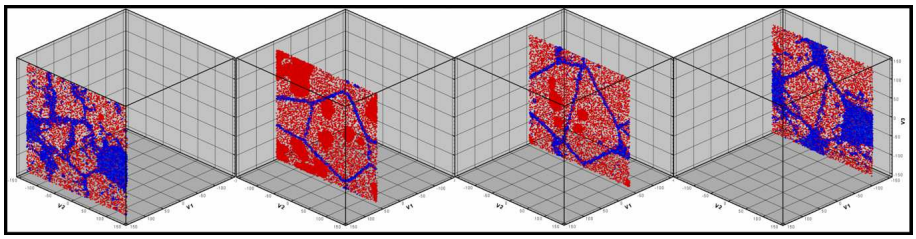

FIG. 7: Four slices of a polycrystalline sample with an average grain size of 5 nm. We observe a multiplicity of configurations of grain boundaries, triple and higher order junctions. Simulation parameters are $x = 0.15$ and $T = 750$ K. Blue dots are Fe atoms sitting at boundaries, red dots are Cr atoms. Fe atoms at perfect bcc positions are not shown. A surprising effect can readily be observed: Cr does not precipitate at any boundaries. Instead all α' precipitates are in the interior of the grains, avoiding contact with the grain boundary network.

in this system based on a classical potential that captures the essentials of its energetics and thermodynamics. The tools developed allow simulations of radiation damage collision cascades, precipitation of saturated solutions, and heterogeneous non-equilibrium processes. We find that this potential predicts an unexpected behavior for the precipitation of the Cr-rich solution, i. e. a rejection of Cr from grain boundaries. Experiments reporting grain boundary Cr depletion [21], presumably due to a kinetic effect (vacancies migrating preferentially via the Cr sites), do not allow one to separate thermodynamics from kinetic effects. *Ab initio* results on free surfaces predict [22] no segregation. Since it is well known that the good corrosion properties of this alloy are due to the increased Cr concentration at the surface, and the formation of oxide, we conclude that in this alloy kinetic and thermodynamic effects both play significant roles in the determination of the microstructure.

In summary FeCr is far from being fully understood, and accurate simulations can only be done if the intricate details of its energetics and thermokinetics are adequately captured. This work represents an step into that direction.

I. APPENDIX I: EMPIRICAL POTENTIALS FOR CONCENTRATED ALLOYS

An elementary treatments of alloys that nonetheless preserves much of their complexity is based on the so called quasi-chemical expression for the energetics of an ensemble of atoms:

$$E = 1/2 \sum_{i,j} \varphi_{i,j} \tag{1}$$

where $\varphi_{i,j} \in \{\varphi_{AA}, \varphi_{AB}, \varphi_{BB}\}$ represents the contribution to the total energy of a bond between atom types AA, AB, or BB, in a binary alloy of A and B species. In a random solid solution of composition x_B, with $x_A + x_B = 1$, where atoms have coordination z, the total energy per atom is given by,

$$e = z/2\{x_A\varphi_{AA} + x_B\varphi_{BB} + x_A x_B \Omega\} \tag{2}$$

with $\Omega = \varphi_{AB} - \{(\varphi_{AA} + \varphi_{BB})/2\}$. Ω measures the departure of the heteroatomic interaction from the average interaction between the species. The heat of formation of the alloy, h.o.f., i. e. the departure of the energy of the alloy with respect to the ideal solution (ideal solution energy is given by the linear interpolation between the pure constituents) is simply given by,

$$\Delta e_f = z/2\{x_A x_B \Omega\} \tag{3}$$

In this model then, the h.o.f., Δe_f, is a quadratic (symmetric) function of composition, with $\Omega > 0$ for solutions showing a tendency to segregate and $\Omega < 0$ for those with tendency to form compounds. The figure shows the energy of the solution versus composition for the 3 possible cases.

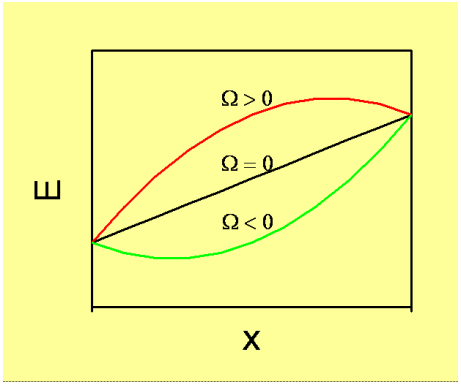

FIG. 8: Energy of a random solid solution in the regular model for different values of Ω

Many solutions in nature do not have a symmetric h.o.f. and therefore additional complexity is usually added to this elementary treatment by introducing a polynomial dependence of Ω on composition, usually called sub regular solution model, using a particular form called the Redlich-Kister expansion,

$$\Omega = \Omega(x_B) = \sum_{p=0}^{n} L_p (1 - 2x_B)^p \tag{4}$$

where L_p are coefficients dependent on temperature. Empirical potentials for molecular dynamics simulations of alloys are built upon expressions similar to the quasi chemical energetics, but with radial dependence and non linear terms. The so-called many body potentials have in common a description of the total energy in terms of the sum over atom energies, themselves composed of two contributions, namely embedding and pair potential terms; it reads,

$$E = \sum_{i}^{N} [F_{\alpha_i}(\sum_{j \neq i} \rho_{\alpha_i \beta_j}(r_{ij})) + 1/2 \sum_{j \neq i} V_{\alpha_i \beta_j}(r_{ij})] \tag{5}$$

where α, β stand for elements A or B sitting at sites i, j; F's are the embedding functions for either type of elements, and V's and ρ's are the pair potentials and densities between α-β pairs. Alloy properties are therefore described by the functions ρ_{AB} and V_{AB}. Depending on the model considered, the density functions do not always include the cross

term ρ_{AB}. Different expressions for the embedding energies, densities, and pair potentials englobe a large diversity of similar models.

From Eq. 5 is appears clearly that the h.o.f. of such an alloy has contributions from the non-linear embedding term and from the pair potential functions. The later provide a contribution to the h.o.f. equivalent to the Ω term in Eq. 2. In order to reproduce complex formation energies, a natural way to add complexity into the model, as suggested by Eq. 4, is to include a composition dependence to the pair potential. This composition has to be a local variable, depending on the environment around atoms i and j (a detailed derivation is given in [17]),

$$E = \sum_{i}^{N}[F_{\alpha_i}(\sum_{j\neq i}\rho_{\alpha_i\beta_j}(r_{ij})) + 1/2\sum_{j\neq i}V_{\alpha_i\beta_j}(x_{i,j}, r_{ij})] \tag{6}$$

$$V_{\alpha_i\beta_j}(x_{i,j}, r_{ij}) = h(x_{i,j})v_{\alpha_i\beta_j}(r_{ij}) \tag{7}$$

For $h(x_{i,j})$ we choose a representation based on the Redlich-Kister expansion of the same order n as needed to fit the h.o.f one wants to model, namely

$$h(x) = \sum_{p}^{n} H_p(1-2x)^p \tag{8}$$

with H_p coefficients obtained by a fitting procedure. This procedure proves to be robust in the sense that given a target h.o.f. is always be possible to find an Embedded Atom type model as given by Eqs. 6 that reproduces it. Figure 9 shows the results for FeCr with the target h.o.f taken from the *ab initio* calculations of Olsson *et al.* [14]. The formation energy is indistinguishable from the target function.

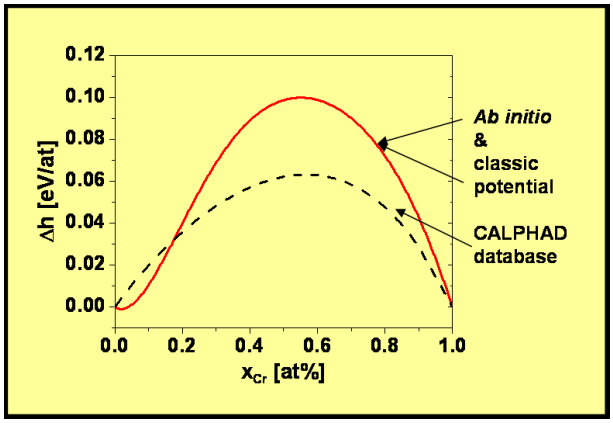

FIG. 9: Heat of formation of a random solid solution of ferromagnetic FeCr as calculated by Olsson et al. [14], as given by the classical potential Eqs. 6, and as reported in CALPHAD database [9]

.

II. APPENDIX II: FROM POTENTIALS TO THERMODYNAMICS

The calculation of the thermodynamic properties of an alloy implies the knowledge of the free energy of the different phases as a function of composition and temperature. The calculation of the free energy is a multi-step process that requires several different molecular dynamics (MD) runs. In recent papers, we implemented a numerical package that allows efficient and accurate calculation of it. For a complete description of the method, we refer the reader to those previous publications [14-16]. Here we only highlight its basic aspects, together with the main equations.

The basic assumption that links thermodynamics to molecular dynamics is ergodicity which assumes that,

$$\overline{A_t} =< A > \tag{9}$$

where the left hand side is a time average in a molecular dynamics run, namely

$$\overline{A_t} = \frac{1}{t-t_0}\int_{t_0}^{t} A(\xi(\tau))d\tau \tag{10}$$

and the right hand side is an ensemble average in the sense of statistical mechanics,

$$< A >= \frac{\int_\Omega A(\xi) exp(-H(\xi)/kT) d\xi}{\int_\Omega exp(-H(\xi)/kT) d\xi} \tag{11}$$

where H is the Hamiltonian of the system, ξ is the ensemble of variables that specify a particular state, k is the Boltzman constant, T is the temperature, and Ω is the volume of the phase space.

Free energy is not an ensemble average, it is rather related to the denominator of Eq. 11,

$$F = -kTln(\int_\Omega exp(-H(\xi)/kT) d\xi) \tag{12}$$

and cannot therefore be obtained as a time average of a MD run. Numerous procedures to calculate free energies have been proposed in the literature, and we refer the reader to our previous work for a detailed discusion [4**?** –8]. We calculate the free energy per particle at a given temperature T, $F(T)$, through a thermodynamic integration between the state of interest and a reference state at temperature T_0 with known free energy $F(T_0)$, using the Gibbs-Duhem equation,

$$F(T) = F(T_0)\frac{T}{T_0} - T\int_{T_0}^{T} \frac{h(\tau)}{\tau^2} d\tau \tag{13}$$

where $h(\tau)$ is the enthalpy per particle. The enthalpy is obtained from a MD run and it is fitted with a polynomial in T, that allows an analytic integration in Eq. 13. The coupling-constant integration method, or switching Hamiltonian method [29], is used to calculate $F(T_0)$. We consider a system with Hamiltonian

$$H = (1-\lambda)W + \lambda U \tag{14}$$

where U describes the actual system (in this work, described with a EAM-type Hamiltonian) and W is the Hamiltonian of the reference system, with known free energy. The parameter λ allows us to switch from U (for $\lambda = 1$) to W (for $\lambda = 0$). With this Hamiltonian we can obtain the free energy difference between W and U by calculating the reversible work required to switch from one system to the other. Then the unknown free energy associated with U, $F(T_0)$, is given by,

$$F(T_0) = F_W(T_0) + \int_0^1 < \frac{\partial H}{\partial \lambda} > d\lambda = F_W(T_0) + \int_0^1 < U - W >_\lambda \, d\lambda \tag{15}$$

where $F_W(T_0)$ is the free energy of the reference system at T_0. The integration is carried over the coupling parameter λ, and $< >$ stands for the average over a canonical ensemble, or a time average in a (T, V, N) constant MD simulation. For the solid phases the reference system W is a set of Einstein oscillators centered on the average positions of the atoms in the (T, $P = 0$, N) ensemble corresponding to the Hamiltonian U. The free energy per atom of the Einstein crystal is known analytically and therefore Eqs. 13 and 15 provide the recipe for free energy calculations.

For alloys the strategy is to construct for each phase of interest a set of free energy functions versus composition x and temperature $F(x, T)$.

In summary, the steps and equations used in this work to obtain free energies and from them phase diagrams are:
- MC generation of solid solution samples in both solid phases.
- MD runs to determine the enthalpy vs T for solid solutions at different compositions and phases.
- Polynomial fits to the enthalpy.
- Analytic integration of the Gibbs-Duhem relations.
- MD simulations of the switching Hamiltonian process to obtain $< U - W >$ at each composition.
- Analytic integration of polynomial fits to $< U - W >$.

The final result for the free energy of the FeCr alloy in the bcc ferromagnetic phase is shown as a surface in Fig 10. Isotherm lines, in black over the surface, are used together with the common tangent construction to determine the phase diagram shown in Fig 4.

Acknowledgments

This work was performed under the auspices of the U.S. Department of Energy by the University of California, Lawrence Livermore National Laboratory under Contract No. W-7405-Eng-48. Support from the LDRD Office is

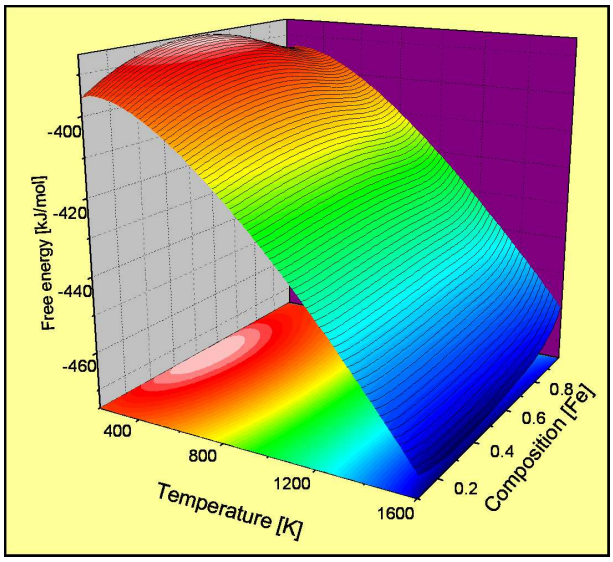

FIG. 10: Free energy of a FeCr random solid solution in the ferromagnetic phase, as a function of temperature T and Fe composition x. Note the anomalous behavior at low T and high x related to the change in sign of the heat of formation (see main text).

acknowledged.

[1] F. A. Garner, M. B. Toloczko, and B. H. Sencer, J. Nucl. Mater. **276**, 123 (2000).
[2] A. Hishinuma, A. Kohyama, R. L. Klueh, D. S. Gelles, W. Dietz, and K. Ehrlich, J. Nucl. Mater. **258-263**, 193 (1998).
[3] S. J. Zinkle, Phys. Plasmas **12**, 058101 (2005).
[4] A. Caro, P. E. A. Turchi, M. Caro, and E. M. Lopasso, J. Nucl. Mater. **336**, 233 (2005).
[5] A. Caro, M. Caro, E. M. Lopasso, P. E. A. Turchi, and D. Farkas (2006).
[6] E. O. Arregui, M. Caro, and A. Caro, Phys. Rev. B **66**, 054201 (2002).
[7] E. M. Lopasso, M. Caro, A. Caro, and P. E. A. Turchi, Phys. Rev. **B 68**, 214205 (2003).
[8] A. Caro, M. Caro, E. M. Lopasso, P. E. A. Turchi, and D. Farkas, Jr. Nuc. Mat. **336**, 233 (2004).
[9] N. Saunders and A. P. Miodownik, *Calphad. A comprehensive guide* (Pergamon Materials Series, R. W. Cahn Editor, 1998).
[10] I. Ansara and B. Sundman, *Computer Handling and Dissemination of Data* (Elsevier Science Pub Co., London, UK, 1987).
[11] A. Dinsdale, CALPHAD **15**, 317 (1991).
[12] M. I. Mendelev, S. Han, D. J. Srolovitz, G. J. Ackland, D. Y. Sun, and M. Asta, Phil. Mag **83**, 3977 (2003).
[13] J. Wallenius, P. Olsson, C. Lagerstedt, N. Sandberg, R. Chakarova, and V. Pontikis, Phys. Rev. **69**, 094103 (2004).
[14] P. Olsson, I. A. Abrikosov, L. Vitos, and J. Wallenius, J. Nucl. Mater. **321**, 84 (2003).
[15] T. P. C. Klaver, R. Drautz, and M. W. Finnis, Phys. Rev. B **74**, 094435 (2006).
[16] A. A. Mirzoev, M. M. Yalalov, and D. A. Mirzaev, The Physics of Metals and Metallography **97**, 336 (2003).
[17] A. Caro, D. A. Crowson, and M. Caro, Phys. Rev. Lett. **95**, 075702 (2005).
[18] Details of this parallel Monte Carlo code will be published elsewhere (????).
[19] V. Barbe and M. Nastar, Nature Mater. **5**, 482 (2006).
[20] B. Sadigh, A. Caro, M. Caro, and E. M. Lopasso, to be published (2006).
[21] E. Wakay and et al., J. Physique **C7**, 277 (1995).
[22] W. T. Geng, Phys. Rev. B **68**, 233402 (2003).